Classification of low level visual texture features based on the Hermite transform

Alfonso Estudillo-Romero* and Boris Escalante-Ramirez§
Universidad Nacional Autonoma de Mexico
Fac. de Ingenieria, Edif. de Posgrado e Investigacion
Ciudad Universitaria, C.P. 04510, Mexico, D.F., Mexico
**aestudillor@uxmcc2.iimas.unam.mx*
§*boris@servidor.unam.mx*

***Abstract*—A biological inspired image analysis technique to extract visual texture features is presented. The Hermite transform describes locally basic image features in terms of Gaussian derivatives. Multiresolution combined with several derivative orders of analysis provides detection of patterns that characterize every texture class. Maximum energy direction analysis and steering of the transformation coefficients increase the method robustness against the texture orientation. Texture features are computed by extracting statistical information from the orientation-invariant visual features and arranged into a compact vector. The PCA technique is used to select the most significant linear combinations of the vector elements to reduce vector dimensionality. We evaluate the correct classification rate for several kinds of texture features with real textures sets and the effects of the number of principal components on the classification performance.**

***Keywords*-texture classification, visual texture features, Hermite transform, image indexing, Content-based image retrieval (CBIR)**

I. Introduction

The increasing media content in a wide range of areas requires automatic methods to browse on large databases to find and retrieve images based on relevant content for the user. Indexing and classification are crucial tasks to obtain high retrieval performances. Browsing medical images for diagnosis aid [1], classification of the quality of a given process in industrial environments [2][3] and indexing of manuscripts [4] are some examples.

In order to obtain useful features for classification and indexing, in this paper we propose a biologically inspired image analysis technique to extract visual texture features regardless the orientation of the input texture.

For texture analysis many techniques have emerged, such as gray-level co-occurrence matrices [5], Markov random field models [6], local binary patterns [7] and, filtered based methods including Gabor filters [8] and different wavelets types [9], [10]. The Gabor filtering based technique has been widely used due to the fact that the Gabor functions are capable to model the receptive field profiles of simple cells of mammalian visual systems. Another reason is their optimal joint resolution in both the space and frequency domains [11].

The Hermite transform is a local decomposition technique that expands an image into orthogonal polynomials with respect to a Gaussian window [12]. One of the advantages of using the Hermite transform over wavelet-based methods is that its analysis functions are similar to Gaussian derivatives. Psycho-visual evidence suggests that the Gaussian derivatives fit the receptive field profiles of mammalian visual systems [13].

In this paper, we present an exhaustive evaluation of the correct classification rate (CCR) of several kinds of common statistical texture features extracted from the orientation invariant visual features. We compare the results with the classification performance obtained after a dimensionality reduction method with principal components analysis (PCA). The effects of the number of principal components (PCs) on the classification rates are also reported. Previous work [14] has shown that the augmented variance ratio (AVR) improves the CCR with a reduced number of feature elements.

Sect. II presents the theoretical foundations of the Hermite transform and its steered version in Sect. III to achieve rotation-invariance. The common statistical texture features that we evaluate are presented in Sect. IV. Section V presents the PCA dimensionality reduction method. Datasets and experimental setups are detailed in Sect. VI. Finally, results and conclusions are given in Sect. VII and VIII respectively.

II. Hermite Transform

A one dimensional polynomial transform $f_n(x)$ locally represents an input signal in terms of a sum of the windowed $V(x)$ input signal $f(x)$ times its orthogonal polynomial $G_n(x)$ at every window position [12]:

$$f_n(x_0) = \int_x f(x) G_n(x_0 - x) V_n^2(x_0 - x) dx \qquad (1)$$

By choosing a Gaussian window

$$V(x) = \frac{1}{\sqrt{\sqrt{\pi}\sigma}} \cdot e^{-x^2/2\sigma^2} \qquad (2)$$

its corresponding orthogonal polynomial are given by the Hermite polynomials $H_n(x)$ [15]:

$$H_n(x) = (-1)^n e^{x^2} \frac{d^n e^{-x^2}}{dx^n}, \quad n = 0, 1, 2, \ldots \qquad (3)$$

978-0-7695-4635-3/11 $26.00 © 2011 IEEE
DOI 10.1109/SITIS.2011.61

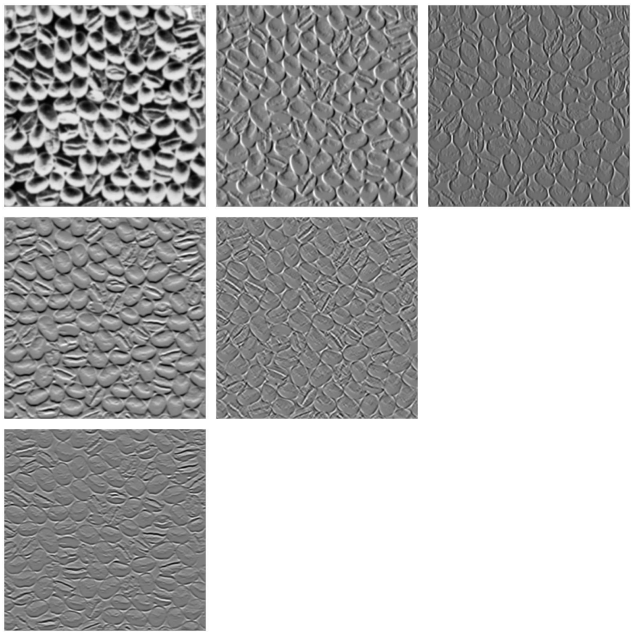

Figure 1. Hermite transform at one scale of analysis. Input texture corresponds to a region from the Brodatz texture D74 [16]

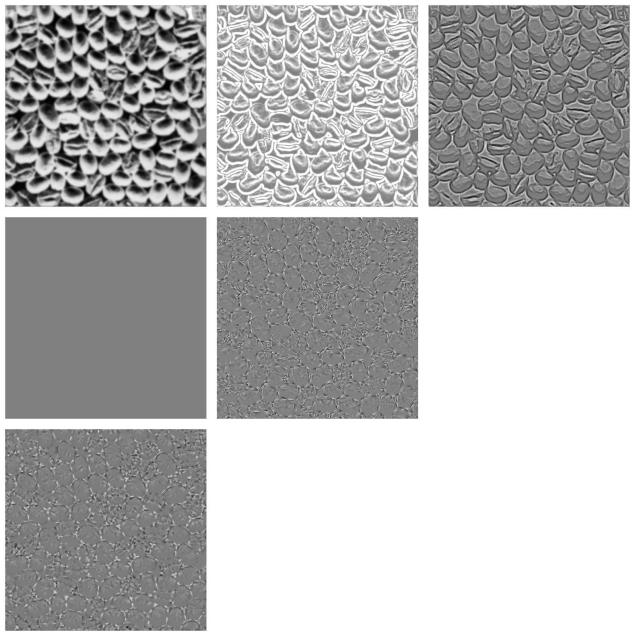

Figure 2. Steered Hermite transform for one scale of analysis. Input texture corresponds to a region from the Brodatz texture D74 [16]

The expansion coefficients $f_n(x)$ are obtained by convolution of the input signal $f(x)$ with the Hermite analysis functions $d_n(x)$ given in terms of the window and the Hermite polynomials as:

$$d_n(x) = \frac{(-1)^n}{\sqrt{2^n n!}} \cdot \frac{1}{\sigma\sqrt{\pi}} H_n\left(\frac{x}{\sigma}\right) e^{-x^2/\sigma^2} \tag{4}$$

Since the analysis functions have the property of being both spatially separable and rotationally symmetric the two dimensional analysis functions are written as:

$$d_{n-m,m}(x,y) = d_{n-m}(x) d_m(y) \tag{5}$$

where $n-m$ and m denote the analysis order in x and y direction respectively. As a result, we can expand a given input image $f(x,y)$ given the 2D analysis function from Eq. 5 as:

$$f_{n-m,m}(x_0,y_0) = \int_x \int_y f(x,y) \cdot d_{n-m,m}(x_0 - x, y_0 - y) dx dy \tag{6}$$

for $n = 0, 1, \ldots, \infty$ and $m = 0, \ldots, n$. Fig. 1 shows the Hermite transform at one scale of analysis. From left to right and from top to bottom the analysis order increases in the x-direction and y-direction respectively.

III. Orientation Invariant Visual Features

Since all Hermite analysis filters are polynomials times a radially symmetric window function, rotated versions of a filter of order n can be constructed by taking linear combinations of the original filters of order n [17], The transformation can be written in terms of the orientation selectivity $\alpha_{n-k,k}(\theta)$ [18]:

$$f^{\theta}_{n-m,m}(x_0,y_0,\theta) = \sum_{k=0}^{n} f_{n-k,k}(x_0,y_0) \alpha_{n-k,k}(\theta) \tag{7}$$

which has been named the steered Hermite transform [19]. The terms $\alpha_{n-m,m}(\theta)$ are the Cartesian angular functions of order n which give such orientation selectivity and are defined as:

$$\alpha_{n-m,m}(\theta) = \sqrt{C_n^m} \cos^{n-m}(\theta) \sin^m(\theta) \tag{8}$$

where C corresponds to a binomial window which approximates the discrete Gaussian window. Fig. 2 shows the steered Hermite transform at one scale of analysis.

The local energy can be written in terms of the steered Hermite coefficients as:

$$E_N = \sum_{n=0}^{N} \sum_{m=0}^{n} [f_{n-m,m}]^2 = \sum_{n=0}^{N} \sum_{m=0}^{n} [f^{\theta}_{n-m,m}]^2 \tag{9}$$

for all $N \geq 0$. One may distinguish 1D local energy terms and 2D local energy terms. Thus, we can split local energy of (9) up to order N as:

$$E_N = [f_{0,0}]^2 + E_N^{1D} + E_N^{2D} \tag{10}$$

where $f_{0,0}$ represents the DC Hermite coefficient and

$$E_N^{1D} = \sum_{n=1}^{N} [f^{\theta}_{n,0}]^2 \tag{11}$$

$$E_N^{2D} = \sum_{n=1}^{N} \sum_{m=1}^{n} [f_{n-m,m}^{\theta}]^2 \tag{12}$$

One of the objectives when steering coefficients is to maximize detection of patterns along a given local direction θ. In this way, [20], [18], [19] propose strategies in which θ is selected such that E_N^{1D} is maximized. Fig. 2 shows the steered Hermite transform at one scale of analysis. Observe that most content of visual information has been compacted on the first row as 1D patterns.

IV. Statistical Texture Features

The CCR was evaluated for several kinds of statistical texture features found in the literature:

1) mean,

$$\mu = \frac{1}{H \times W} \sum_{w=1}^{W} \sum_{h=1}^{H} f_{n,0}^{\theta} \tag{13}$$

2) standard deviation,

$$\sigma = \sqrt{\frac{1}{(H \times W - 1)} \sum_{w=1}^{W} \sum_{h=1}^{H} [f_{n,0}^{\theta} - \mu]^2} \tag{14}$$

3) and energy features

$$E_0 = \sum_{w=1}^{W} \sum_{h=1}^{H} [f_{n,0}^{\theta}]^2 \tag{15}$$

$$E_1 = \frac{E_0}{H \times W} \tag{16}$$

$$E_2 = \frac{1}{H \times W} \sum_{w=1}^{W} \sum_{h=1}^{H} |f_{n,0}^{\theta}| \tag{17}$$

$$E_3 = \frac{1}{H \times W} \sum_{w=1}^{W} \sum_{h=1}^{H} \sqrt{|f_{n,0}^{\theta}|} \tag{18}$$

where H and W are the dimensions of the steered Hermite coefficients.

For every one of the texture features described above, a feature vector $\mathbf{x}$ is obtained by concatenating the extracted features x_j from the steered Hermite coefficients of order n at every scale of analysis s. Note that the analysis order is given by $1 \leq n \leq N$ up to order N and the scales of analysis by $1 \leq s \leq S$. Thus, the vector size is $S \times N$.

V. Principal Components Analysis

The principal components analysis (PCA) technique, also know as the Karhunen Loeve (KL) transform or the Hotelling transform, is based on factorization techniques developed in linear algebra. PCA can be seen as a transformation of the original dataset into a new vector space spanned by basis functions that decompose the data in decreasing order energy components. In order to reduce dimensionality or compress original data the minor energy components may be eliminated. Many classification schemes work in this space in order to achieve better separability.

Let $\mathbf{X}$ represent a set of m vectors or measures:

$$\mathbf{X} = \{\mathbf{x}_1, \mathbf{x}_2, \ldots, \mathbf{x}_m\} \tag{19}$$

whose vectors $\mathbf{x}_i$ have n elements each one. From now and on we name such elements, features:

$$\mathbf{x}_i = \{x_{i,1}, x_{i,2}, \ldots, x_{i,n}\} \tag{20}$$

We can group all the features in a feature matrix $\mathbf{F_X}$ as:

$$\mathbf{F_X} = \begin{bmatrix} x_{1,1} & x_{1,2} & \ldots & x_{1,n} \\ x_{2,1} & x_{2,2} & \ldots & x_{2,n} \\ \vdots & \vdots & \vdots & \vdots \\ x_{m,1} & x_{m,2} & \ldots & x_{m,n} \end{bmatrix} \tag{21}$$

where n and m are the number of features and measures respectively. The idea behind PCA is to highlight data that produce maxima variations measured by the covariance matrix defined as:

$$\Sigma_{\mathbf{X}} = \begin{bmatrix} \sigma_{1,1} & \sigma_{1,2} & \ldots & \sigma_{1,n} \\ \sigma_{2,1} & \sigma_{2,2} & \ldots & \sigma_{2,n} \\ \vdots & \vdots & \vdots & \vdots \\ \sigma_{n,1} & \sigma_{n,2} & \ldots & \sigma_{n,n} \end{bmatrix} \tag{22}$$

with $\sigma_{i,j}$ being the covariance between features i and j. The objective of PCA is to transform the data in a way that the covariance matrix becomes diagonal.

In order to transform each feature vector defined in the set $\mathbf{X}$ into another feature vector defined in the new set $\mathbf{Y}$ we look for a transformation $\mathbf{W}$, such that the covariance matrix of the elements in $\mathbf{Y}$ is diagonal. The transformation is linear and it is defined as:

$$\mathbf{F_Y} = \mathbf{F_X} \mathbf{W}^T \tag{23}$$

To obtain the covariance of the features in $\mathbf{Y}$ based on the features in $\mathbf{X}$, such that $\Sigma_{\mathbf{Y}}$ is diagonal we can use the following equation:

$$\Sigma_{\mathbf{Y}} = \mathbf{W} \Sigma_{\mathbf{X}} \mathbf{W}^T \tag{24}$$

By performing some basic liner algebra operations we can find the matrix transformation $\mathbf{W}$ by solving the following equation [21]:

$$(\lambda_i \mathbf{I} - \Sigma_{\mathbf{X}}) \mathbf{w}_i = 0 \tag{25}$$

where $\mathbf{w}_i$ are the rows of $\mathbf{W}$, λ_i and $\mathbf{w}_i$ define the eigenvalues and eigenvectors respectively and $\mathbf{I}$ is the identity matrix. The characteristic equation $\det(\lambda_i \mathbf{I} - \Sigma_{\mathbf{X}}) = 0$ is used to solve for the values of λ_i and consequently obtain $\mathbf{w}_i$ from Eq. 25.

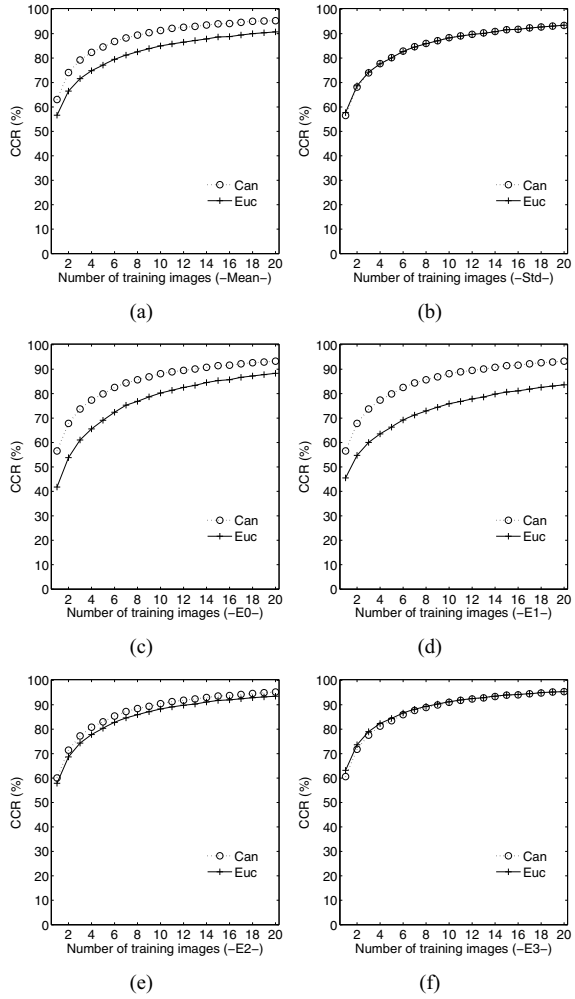

Figure 3. Comparison of CCRs obtained with the Euclidean and Canberra distances for several number of training textures for: a)μ, b)σ, c) E_0, d) E_1, e)E_2, f) E_3 for dataset I.

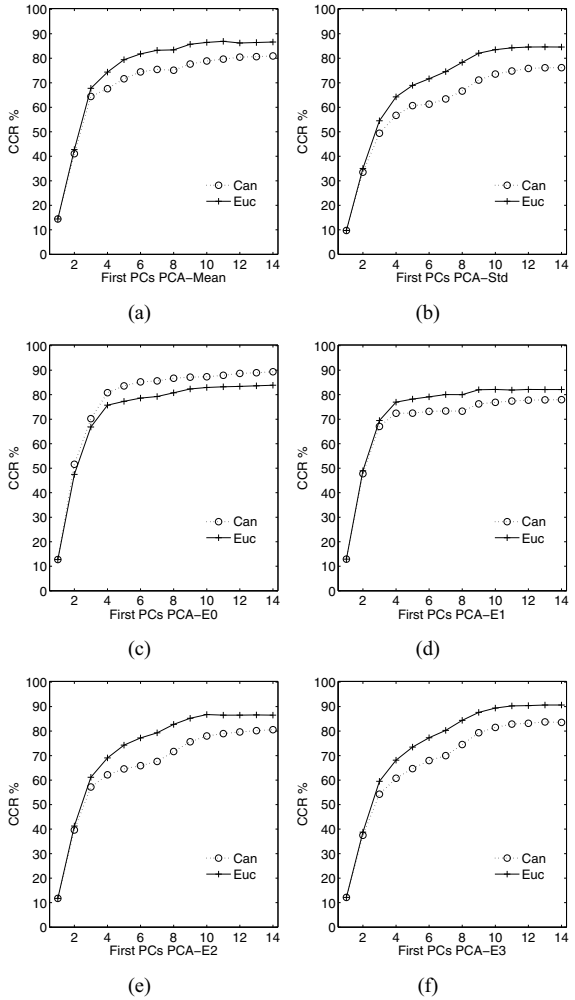

Figure 4. Comparison of CCRs obtained with the Euclidean and Canberra distances after PCA using 14 principal components with 16 training texture images for: a)μ, b)σ, c) E_0, d) E_1, e)E_2, f) E_3 for dataset I.

VI. Datasets and Experimental Setup

We evaluated our proposal by computing the CCRs using two different real textures datasets. For each dataset, the testing and training texture subsets were randomly selected. The CCR was evaluated from 1 to 20 randomly selected training texture images. This evaluation was repeated over 80 trials and therefore possible biasing due to the subset selection was compensated. A comparison between the CCR before and after PCA is also presented for each dataset. We investigate the effects of the number of principal components on the CCR performance.

In all the experiments the training textures were analyzed at $S = 4$ resolution levels with the Hermite transform up to order $N = 8$, yielding a feature vector of 32 arranged elements. Further steering of the Hermite transform coefficients compensated the texture orientation changes.

A. Classifier

We evaluated classification accuracy based on the k-NN classifier using two distance measurements. Given two feature vectors $\mathbf{x}$ and $\mathbf{y}$ of n features, then the Euclidean distance is defined as:

$$d_E(\mathbf{x},\mathbf{y}) = \sqrt{\sum_{j=1}^{n}(x_j - y_j)^2} \tag{26}$$

and the Canberra distance as:

$$d_C(\mathbf{x},\mathbf{y}) = \sum_{j=1}^{n}\frac{|x_j - y_j|}{|x_j| + |y_j|} \tag{27}$$

Classification accuracy is measured by computing the CCR defined as:

$$\text{CCR} = \frac{N_c}{N_{Te}} \tag{28}$$

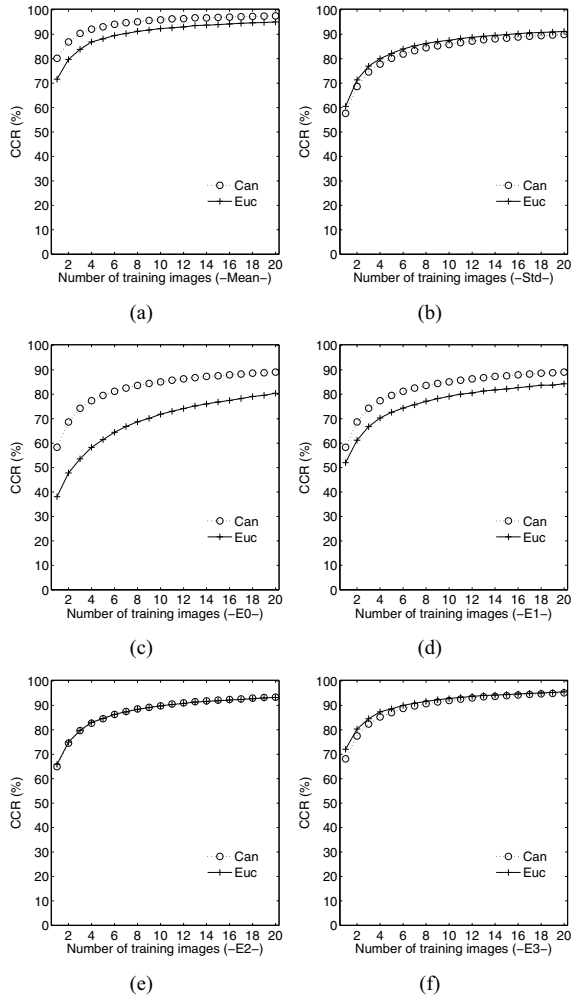

Figure 5. Comparison of CCRs obtained with the Euclidean and Canberra distances for several number of training textures for: a)μ, b)σ, c) E_0, d) E_1, e)E_2, f) E_3 for dataset II.

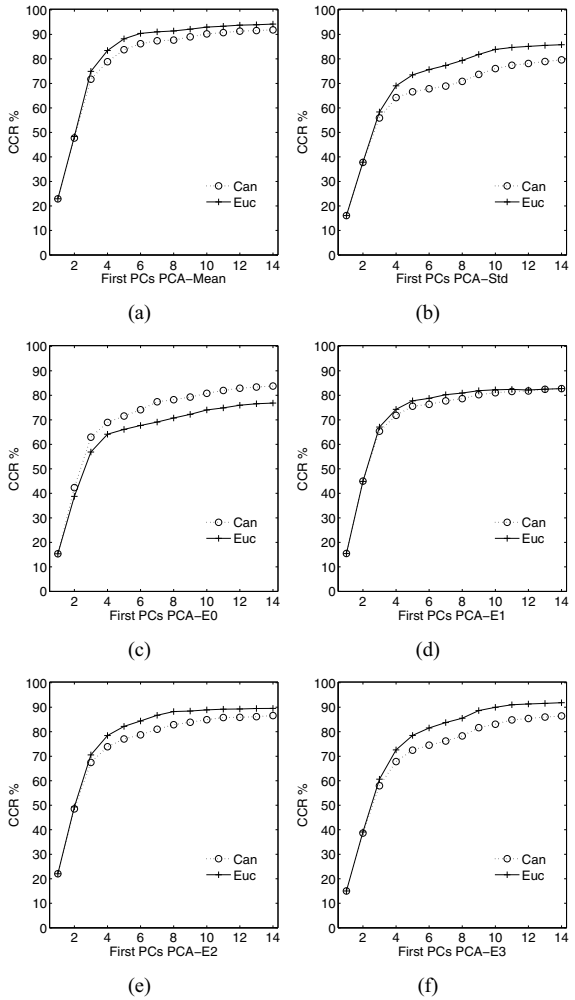

Figure 6. Comparison of CCRs obtained with the Euclidean and Canberra distances after PCA using 14 principal components with 16 training texture images for: a)μ, b)σ, c) E_0, d) E_1, e)E_2, f) E_3 for dataset II.

where N_c is the number of testing images that were correctly classified and N_{Te} is the number of testing images.

B. Dataset I

It consists of 54 texture images of 512×512 pixels from the VisTex texture database [22] as was proposed in [23]. The texture classes that were used are coded in the VisTex database as: *Bark.0000*, *Bark.0001*, *Bark.0003*, *Bark.0005*, *Bark.0006*, *Bark.0007*, *Bark.0008*, *Bark.0010*, *Brick.0000*, *Brick.0002*, *Brick.0004*, *Brick.0005*, *Buildings.0003*, *Buildings.0009*, *Fabric.0000*, *Fabric.0002*, *Fabric.0004*, *Fabric.0008*, *Fabric.0011*, *Fabric.0014*, *Fabric.0015*, *Fabric.0017*, *Flowers.0000*, *Flowers.0003*, *Flowers.0005*, *Food.0001*, *Food.0003*, *Food.0005*, *Food.0008*, *Grass.0002*, *Leaves.0000*, *Leaves.0002*, *Leaves.0003*, *Leaves.0006*, *Leaves.0010*, *Leaves.0013*, *Leaves.0014*, *Leaves.0016*, *Metal.0000*, *Metal.0002*, *Metal.0004*, *Misc.0001*, *Misc.0002*, *Sand.0002*, *Sand.0005*, *Stone.0002*, *Stone.0004*, *Terrain.0010*, *Tile.0001*, *Tile.0007*, *Water.0000*, *Water.0004*, *Water.0006*, *Wood.0002*.

The dataset was formed by first artificially rotation of each texture image from 0 to $16\pi/18$ radians with incremental steps of $\pi/18$ radians, thus 17 rotation angles. Then 4 sub-images of 128×128 pixels without overlap were extracted from each rotated texture image in such a way that the sub-images had minimal overlap between the different rotated versions. Thus, $54 \times 17 \times 4 = 3672$ comprises the size of the texture dataset.

C. Dataset II

This dataset consists of 24 texture images of 538×746 pixels from the Outex texture database (available on line at http://www.outex.oulu.fi) as was proposed in [7]. The texture classes that were used are coded in the Outex database as:

canvas001, *canvas002*, *canvas003*, *canvas005*, *canvas006*, *canvas009*, *canvas011*, *canvas021*, *canvas022*, *canvas023*, *canvas025*, *canvas026*, *canvas031*, *canvas032*, *canvas033*, *canvas035*, *canvas038*, *canvas039*, *tile005*, *tile006*, *carpet002*, *carpet004*, *carpet005* and *carpet009*.

The texture images were acquired with incandescent illumination, named as "inca" in the Outex database, at 100 dpi spatial resolution. The textures were naturally rotated with nine rotation angles (0°, 5°, 10°, 15°, 30°, 45°, 60°, 75° and 90°). The 24-bit RGB images were transformed into eight bit intensity images using:

$$I = 0.299R + 0.587G + 0.114B \tag{29}$$

The dataset was formed from 20 non-overlapping texture samples of size 128×128 pixels from each intensity texture image. Thus, $24 \times 9 \times 20 = 4320$ comprises the size of the texture dataset.

VII. Results

Figs. 3 and 5 show the classification results without PCA for datasets I and II respectively. The Canberra distance performed the best CCRs in all experiments and similar to the Euclidean distance in the worst cases for both datasets without dimensionality reduction by means of PCA. For both datasets, the features μ, E_2 and E_3 obtained the best classification results.

From plots in Figs. 3 and 5 it is possible to observe that a small number of training textures are enough to obtain good CCRs. This is of prime importance since real recognition and classification tasks frequently have small training sets.

In order to investigate the effects of the number of principal components (PCs) on the CCRs performances, we first fixed 16 and 20 training texture images for the first and second datasets respectively.

In Figs. 4 and 6 we show the CCRs obtained after PCA by varying the number of PCs from 1 to 14 for datasets I and II respectively. As shown, stable CCRs were obtained starting from 10 PCs. This represents an advantage for storage and similarity computation of the texture feature vectors.

Comparisons of CCRs are summarized in Tables I and II for datasets I and II respectively. After selecting 14 PCs with the PCA technique, the Euclidean distance performed the best CCRs in all experiments except for E_0. For both datasets, the features μ, E_2 and E_3 obtained the best classification results.

We observed that the PCA technique do not improves the CCRs. Nevertheless good approximations are obtained with a small number of PCs.

VIII. Conclusion

Texture feature extraction was performed by considering visual information by means of the analysis functions of the Hermite transform. Visual details were then locally described as rotational invariant texture patterns. The comparative evaluations of several kinds of texture features have shown better CCRs performances for the statistical texture features such as, μ, E_2 and E_3.

Multiple evaluations from randomly training and testing subsets allowed to obtain average CCRs with no dependence on the sets configuration. Using the PCA technique good CCRs were obtained with a small number of training texture images and principal components although no CCRs improvements were observed.

Table I
Comparison of CCRs (%) for dataset I using 16 training texture images

Feature	32-Features	14-PCs
μCan	94.13	80.93
μEuc	88.80	86.64
σCan	91.76	76.17
σEuc	91.76	84.60
E_0Can	91.65	89.39
E_0Euc	85.71	83.89
E_1Can	91.65	77.98
E_1Euc	81.14	82.10
E_2Can	93.78	80.60
E_2Euc	92.00	86.52
E_3Can	94.07	83.56
E_3Euc	94.18	90.64

Table II
Comparison of CCRs (%) for dataset II using 20 training texture images

Feature	32-Features	14-PCs
μCan	97.50	91.84
μEuc	95.07	94.21
σCan	89.94	79.61
σEuc	91.17	85.79
E_0Can	89.08	83.80
E_0Euc	80.43	76.86
E_1Can	89.08	82.76
E_1Euc	84.30	82.75
E_2Can	93.39	86.59
E_2Euc	93.24	89.55
E_3Can	95.14	86.42
E_3Euc	95.53	91.94

Acknowledgment

This work was supported by UNAM grants PAPIIT IN113611 and IXTLI IX100610

References

[1] G. Quellec, M. Lamard, G. Cazuguel, B. Cochener, and C. Roux, "Wavelet optimization for content-based image retrieval in medical databases," *Medical Image Analysis*, vol. 14, no. 2, pp. 227–241, 2010.

[2] S. Arivazhagan, L. Ganesan, and S. Bama, "Fault segmentation in fabric images using Gabor wavelet transform," *Machine Vision and Applications*, vol. 16, no. 6, pp. 356–363, 2006.

[3] L. Liu, M. Ngadi, S. Prasher, and C. Gariépy, "Categorization of pork quality using gabor filter-based hyperspectral imaging technology," *Journal of Food Engineering*, vol. 99, no. 3, pp. 284–293, 2010.

[4] S. Bres, V. Eglin, and C. Rivero, "Handwriting documents denoising and indexing using hermite transform," in *Pattern Recognition and Data Mining*, ser. LNCS, vol. 3686, 2005, pp. 664–673.

[5] R. Haralick, "Statistical and structural approaches to texture," *Proceedings of the IEEE*, vol. 67, no. 5, pp. 786–804, 1979.

[6] G. R. Cross and A. K. Jain, "Markov random field texture models," *IEEE Trans. PAMI*, vol. 5, no. 1, pp. 25–39, 1983.

[7] T. Ojala, M. Pietikäinen, and T. Mäenpää, "Multiresolution gray-scale and rotation invariant texture classification with local binary patterns," *IEEE Trans. PAMI*, vol. 24, no. 7, pp. 971–987, 2002.

[8] A. C. Bovik, M. Clark, and W. S. Geisler, "Multichannel texture analysis using localized spatial filters," *IEEE Trans. PAMI*, vol. 12, no. 1, pp. 55–73, 1990.

[9] C.-M. Pun and M.-C. Lee, "Log-polar wavelet energy signatures for rotation and scale invariant texture classification," *IEEE Trans. PAMI*, vol. 25, no. 5, pp. 590–603, 2003.

[10] R. Manthalkar, P. K. Biswas, and B. N. Chatterji, "Rotation and scale invariant texture features using discrete wavelet packet transform," *Pattern Recognition Letters*, vol. 24, no. 14, pp. 2455–2462, 2003.

[11] J. G. Daugman, "Uncertainty relation for resolution in space, spatialfrequency, and orientation optimized by two-dimensional visual cortical filters," *J. Opt. Soc. Am.*, vol. A 2, no. 7, pp. 1160–1169, 1985.

[12] J.-B. Martens, "The hermite transform-theory," *IEEE Transactions on Acoustics, Speech and Signal Processing*, vol. 38, no. 9, pp. 1595–1606, 1990.

[13] R. A. Young, "Orthogonal basis functions for form vision derived from eigenvector analysis," in *ARVO Abstracts*. Sarasota, FL: Association for Research in Vision and Ophthalmology, Abstract, 1978, p. 22.

[14] A. Estudillo-Romero and B. Escalante-Ramirez, "Rotation-invariant texture features from the steered hermite transform," *Pattern Recognition Letters*, in press, doi:1016/j.patrec.2011.06.014.

[15] M. Abramowitz and I. Stegun, *Handbook of Mathematical Functions*. Dover, 1965.

[16] P. Brodatz, *Texture: a photographic album for artists and designers*. New York: Dover, 1966.

[17] W. Freeman and E. Adelson, "The design and use of steerable filters," *IEEE Trans. PAMI*, vol. 13, no. 9, pp. 891–906, 1991.

[18] J. Silvan-Cardenas and B. Escalante-Ramirez, "The multiscale hermite transform for local orientation analysis," *IEEE Transactions on Image Processing*, vol. 15, no. 5, pp. 1236–1253, 2006.

[19] A. M. van Dijk and J.-B. Martens, "Image representation and compression with steered hermite transforms," *Signal Processing*, vol. 56, no. 1, pp. 1–16, 1997.

[20] J.-B. Martens, "The Hermite transform: a survey," *EURASIP Journal of Applied Signal Processing*, vol. 26145, pp. 1110–8657, 2006.

[21] M. S. Nixon and A. S. Aguado, *Feature Extraction and Image Processing*, 2nd ed. Academic Press, 2008.

[22] VisTex, "Mit media lab vision textures," 2002. [Online]. Available: http://vismod.media.mit.edu

[23] W. Pan, T. D. Bui, and C. Y. Suen, "Rotation invariant texture classification by ridgelet transform and frequency-orientation space decomposition," *Signal Processing*, vol. 88, no. 1, pp. 189–199, 2008.